AIAA'88

AIAA-88-0237
Structure and Mixing Properties of Pressure-Atomized Sprays

G. A. Ruff, A. D. Sagar, and G. M. Faeth, The University of Michigan, Ann Arbor, MI

AIAA 26th Aerospace Sciences Meeting
January 11-14, 1988/Reno, Nevada

Structure and Mixing Properties of Pressure-Atomized Sprays

G. A. Ruff[*], A. D. Sagar[†], and G. M. Faeth[‡]

The University of Michigan, Ann Arbor, Michigan

Abstract

A theoretical and experimental study of the dense-spray region of pressure-atomized nonevaporating sprays is described, emphasizing flows in the wind-induced and atomization breakup regimes. Mean and fluctuating velocities at the injector exit, mean liquid volume fraction distributions, and entrainment rates were measured for large-scale (9.5 and 19.1 mm injector diameters) water jets in still air at atmospheric pressure. It was found that mixing was strongly influenced by the degree of flow development at the injector exit and the breakup regime: fully-developed injector flow and atomization breakup yielded the fastest mixing rates. Predictions based on the locally-homogeneous flow approximation, where relative velocities between the phases are neglected, gave encouraging predictions of dense spray properties in the near-injector region for atomization breakup, including representation of flow development effects at the injector exit.

Nomenclature

d	=	injector exit diameter
f	=	mixture fraction
g	=	square of mixture fraction fluctuations
k	=	turbulence kinetic energy
L	=	injector passage length
Oh	=	Ohnesorge number
r	=	radial distance
Re	=	Reynolds number
u	=	streamwise velocity
v	=	radial velocity
w	=	tangential velocity
We	=	Weber number
x	=	streamwise distance
α	=	volume fraction
ε	=	rate of dissipation of turbulence kinetic energy
μ	=	molecular viscosity
ρ	=	density
σ	=	surface tension

Subscripts

c	=	centerline value
f	=	liquid-phase property
g	=	gas-phase property
o	=	injector exit condition

Superscripts

$(\bar{\ }),(\bar{\ })'$	=	time-averaged mean and root-mean-squared fluctuating quantities
$(\tilde{\ }),(\tilde{\ })''$	=	Favre-averaged mean and root-mean-squared fluctuating quantities

[*]Graduate Assistant, Aerospace Engineering.

[†]Graduate Assistant, Aerospace Engineering; currently at Materials Science and Engineering Department, MIT, Cambridge, MA.

[‡]Professor, Aerospace Engineering; Associate Fellow, AIAA.

Introduction

Liquid injection into a gas is an important fundamental flow, since it is the multiphase counterpart of the single-phase jet. This flow also has practical applications for pressure-atomized sprays, which are common in propulsion and power systems, e.g., pressure atomization is used for fuel or propellant injectors of afterburners, liquid rocket engines, and fuel-injected internal combustion engines. Motivated by these observations, the present investigation considered the dense-spray region of nonevaporating pressure-atomized sprays in a still environment. Spray structure was measured in the near-injector region, to gain a better understanding of breakup and mixing properties of the flow. The new measurements were also used to evaluate analysis of the flow, based on the locally-homogeneous flow (LHF) approximation of multiphase flow theory, i.e., assuming that interphase momentum transport rates are infinitely fast, so that both phases have the same instantaneous velocity and are in thermodynamic equilibrium at each point in the flow.

The properties of pressure-atomized sprays are strongly influenced by their breakup regime. As injector flow rates increase, the flow passes through a succession of breakup regimes, as follows:[1,2] drip, Rayleigh, first wind-induced, second wind-induced and atomization. Drip breakup involves interactions between surface tension and gravity since fluid inertia is negligible in this regime: large drops are formed at the injector exit which then fall as a single stream. Rayleigh breakup involves interactions between fluid inertia and surface tension: drops having diameters greater than the injector diameter, are formed at some distance from the injector. Wind-induced breakup involves instabilities caused by the relative motion of the gas and the liquid, stabilized by surface tension. First wind-induced breakup is caused by instability of the whole liquid column: drops having diameters comparable to the injector diameter are formed, far from the injector. Second wind-induced breakup involves surface instabilities of the liquid column: drops having diameters much smaller than the injector diameter are formed, beginning at various distances from the injector. The point of break-up moves progressively toward the injector exit as jet velocities increase in the second

wind-induced breakup regime. The atomization breakup regime begins when the point of breakup reaches the injector exit, and persists for all higher injector velocities. The present study was limited to wind-induced and atomization breakup, since these regimes are most important for practical applications, e.g., the other regimes are limited to a narrow range of low injector flow rates.

A pressure-atomized spray has several flow regions during atomization breakup, as follows: a single-phase liquid flow in the injector passage; a dilute-spray region, involving roughly spherical drops with liquid volume fractions less than 1-10 percent, at the periphery of the spray and far from the injector; and a dense-spray region, in the core of the flow near the injector exit. The dense-spray region contains a contiguous all-liquid core, similar to the potential core of a single-phase jet, which is surrounded by a shear layer containing drops, ligaments, and other irregularly-shaped liquid elements. Aside from these general features, however, the properties of the dense-spray region are not well known, due to problems of flow visualization and the limited reliability of probe measurements when liquid volume fractions are high. Even past measurements of the length of the all-liquid core are widely scattered and controversial.[3-5]

Separated-flow analysis has proven to be effective, and is under active development, for dilute sprays.[6,7] Since dense sprays involve liquid elements having complex and unknown shapes and, strong interactions between liquid elements, separated-flow analysis is hard to formulate precisely and has not attracted much attention for analyzing these flows. Thus LHF analysis of dense sprays has been studied as an alternative, although its effectiveness is controversial. Wu et al.[8,9] report measurements of spray angles and drop velocities in nonevaporating pressure-atomized sprays at elevated pressures: concluding that use of the LHF approximation is appropriate for these conditions. On the other hand, Mao et al.[10] found that LHF analysis of combusting pressure-atomized sprays at high pressures gave useful qualitative information, but only had limited quantitative accuracy, due to significant drop inertia in the rapidly decelerating flow field of typical sprays. Experimental evidence on both sides of the controversy, however, came from regions where the spray was actually dilute and is not very convincing. This further complicates the issue, since detailed measurements of the structure of dilute sprays generally show that LHF analysis overestimates rates of flow development and is less effective than separated-flow methods.[11-14]

The present investigation was undertaken to help resolve these controversies concerning the structure of the dense-spray region of pressure-atomized sprays, and the effectiveness of the LHF approximation of estimating the properties of this flow. Measurements of mean liquid volume fractions, using gamma-ray absorption, and entrainment, using laser-Doppler anemometry (LDA), were used to provide information concerning the structure and mixing properties of the dense-spray region. Both techniques avoid problems of obscuration of optical diagnostics and uncertainties of probe measurements at high liquid volume fractions. Predictions of spray structure,

using existing methods of LHF analysis,[7] were also evaluated using the new measurements.

The paper begins with a description of experimental and theoretical methods. Flow visualization is then used to identify breakup regimes and physical phenomena of interest. The paper concludes with discussion of the liquid volume fraction and entrainment measurements, and their comparison with predictions based on the LHF approximation. The following description of is brief, more details are reported elsewhere.[15]

Experimental Methods

Apparatus

Issues being studied relate to the dynamics of turbulent spray mixing processes, which are not thought to be strongly influenced by the injector diameter; therefore, large-scale (9.5 and 19.1 mm diameter) injector passages were used to get adequate spatial resolution for the measurements. Water was used as the test liquid, injected vertically downward in still air at normal temperature and pressure. The water was collected in a baffled tub, to prevent splashing up into the area where measurements were made, and discharged to a drain. City water was supplied to the injector using a centrifugal pump. The rate of water flow was adjusted, using a bypass system; and measured, using a turbine flow meter which was calibrated by collecting water for timed intervals.

Three injectors were used: a slug-flow injector having an exit diameter of 9.5 mm; and two fully-developed flow injectors having diameters of 9.5 and 19.1 mm. The slug-flow injector consisted of a honeycomb flow straightener (1.6 mm cells, 25 mm long) and two screens to calm the flow (16 × 16 square mesh, 0.18 mm diameter wire) followed by a 13.6:1 area contraction to the injector exit. The contraction followed the contour prescribed by Smith and Wang,[16] to obtain a uniform (slug) flow having low turbulence intensities, at the exit. The fully-developed flow injectors used the same flow straightener followed by constant diameter passages having lengths of 41 passage diameters. Instrumentation was mounted rigidly; therefore, flow structure was measured by traversing the injectors horizontally (up to 1 m, with a positioning accuracy of 5 μm) and vertically (up to 2m, with a positioning accuracy of 0.5 mm).

Instrumentation

Flow Visualization. Flash photography was used to study the appearance of the sprays, based on a Xenon Corp., High-Intensity Micropulse System (Model 457A) which provided a 10J light pulse with a 1 μs duration. The photographs were obtained in a darkened room with the flash lamp controlling the time of exposure, using a 4 × 5 Speed Graphic camera loaded with Polaroid, Type 57 black and white film (ASA 3000). The camera was directed normal to the spray axis, from a position near the flash lamp. The sprays were photographed in 250 mm long sections, in order to provide reasonable spatial resolution.

Gamma-Ray Absorption. Distributions of mean liquid volume fractions were measured using gamma-ray absorption. An iodine 125 isotope source (2mCi, emitting primarily at 27.47 keV) provided a soft gamma-ray source which had good absorption levels in order to minimize experimental uncertainties. The source was placed in a lead casket having a collimating aperture with a diameter of 1.6 mm and a length of 13 mm. Gamma rays passing through the flow were detected and counted with a Bicron X-ray probe (Model 1 × M.040/1.54) and an EG&G Ortec single-channel analyzer and counter/timer (Models 556, 590A, 974). A lead aperture (1.5-6 mm in diameter, depending on position, and 12 mm long) was placed in front of the detector, in order to define the path observed through the flow. The energy window of the analyzer was centered at 27.5 keV to minimize spurious counts due to background radiation and Compton scattering (the latter effect, however, is small for the present energy range).

Absorption measurements (based on roughly 25,000 counts) were made for 30-60 parallel paths through the flow, and deconvoluted following Santoro et al.[17] to yield radial distributions of void fraction. Gomi and Hasegawa[18] point out that this technique has fundamental uncertainties depending on whether parallel or normal liquid laminae are assumed, however, the narrow absorption paths used during present measurements reduced this effect to less than 5 percent. The measurements were calibrated using both water cells and the near-injector region of smooth liquid jets at low flow rates. Experimental uncertainties were largely due to finite sampling times, and are estimated (95 percent confidence) to be less than 5 percent for centerline mean liquid volume fractions, and proportionately higher elsewhere.

Laser-Doppler Anemometry. Mean and fluctuating liquid velocities at the injector exit, and mean entrainment rates, were measured using LDA. The green line (514.5 nm) of an argon-ion laser (4W, Coherent, INNOVA 90-4) was used in a dual-beam, frequency-shifted (40 MHz Bragg cell, TSI model 9180-12) arrangement, to eliminate effects of directional bias and ambiguity. The LDA signal was collected using a photomultiplier (TSI Model 9160) and processed using a burst counter (TSI Model 1990C). All measurements involved low burst densities (one scattering particle in the measuring volume) and high data densities (time between validated signals small in comparison to integral time scales); therefore, the analog output of the processor was time-averaged to yield unbiased time averages.

LDA measurements of injector exit conditions were obtained for injection into a water-filled windowed chamber. The initial beam spacing was 50 mm, sending and receiving optics had 250 mm focal lengths, and signal detection was 30 deg off axis in the forward-scattering direction. This yielded a measuring volume having a diameter of 110 μm and a length of 220 μm, which was positioned in a plane 0.1 injector diameters from the injector exit. The local water supply contained adequate natural seeding. Streamwise and radial velocities were measured by orienting the laser beam plane appropriately. Experimental uncertainties (95 percent confidence) were largely

governed by finite sampling times, and were less than 5 percent for mean velocities and 10 percent for fluctuating velocities, at the axis, and proportionately higher elsewhere.

The only change in the optical configuration for the entrainment measurements was the use of 600 mm focal length sending and receiving optics, yielding a measuring volume having a diameter of 260 μm and a length of 520 μm. Mean streamwise and radial entrainment velocities were measured near the edge of the flow, with the entire test cell seeded with condensed bay oil particles (ca. 1 μm diameter). These measurements were integrated to provide entrainment rates, with experimental uncertainties (95 percent confidence) estimated to be less than 25 percent.

Test Conditions. Test conditions are summarized in Table 1. Three conditions were examined for each injector, corresponding to first wind-induced, second wind-induced, and atomization breakup. These determinations were based on present observations of the flows. Ranz[1] suggests $We_f > 8$ and $0.4 < We_g < 13$ for wind-induced breakup; and $We_f > 8$ and $We_g > 13$ for atomization; while Miesse[19] suggests $We_g > 40.3$ for atomization. The results of Table 1 are in rough accord with these criteria, even though present injectors are an order of magnitude larger than those used by Ranz[1] and Miesse.[19] The main difference is that the present second wind-induced conditions are slightly beyond the estimated transitions to atomization; however, in these cases, breakup was relatively close to the injector (x/d ~ 3) and was not far removed from atomization conditions.

Table 1. Test Conditions[a]

Breakup Regime	Flow Rate (kg/s)	Injector Pressure Drop (kPa)	Re_f × 10^{-5}	We_g	We_f × 10^{-3}
9.5 mm diameter, fully-developed and slug flow, $Oh = 12.1 \times 10^{-4}$:					
1st Wind-Induced	0.39	80	0.52	4.6	3.9
2nd Wind-Induced	1.55	420	2.07	72.9	61.9
Atomization	3.99	2520	5.34	492.8	419.0
19.1 mm diameter, fully-developed flow, $Oh = 8.6 \times 10^{-4}$:					
1st Wind-Induced	1.32	30	0.88	6.6	5.6
2nd Wind-Induced	4.50	360	3.00	76.7	65.2
Atomization	11.00	2070	7.32	458.6	389.9

[a]Pressure-atomized water injected vertically downward in still air at 98.8 kPa, 298 ± 2K, with a constant-area passage 41 diameters long for fully developed flow: $Re_f = \rho_f u_0 d / \mu_f$, $We_i = \rho_i u_0^2 d / \sigma$, $Oh = \mu_f / (\rho_f d \sigma)^{1/2}$.

Theoretical Methods

<u>General Description</u>

The LHF analysis was similar to past work in this laboratory,[6,7] aside from changes needed to treat the specifics of water injection into air. In addition to the LHF approximation, the major assumptions of the analysis are as follows: steady (in the mean) axisymmetric flow with no swirl; boundary-layer approximations apply; negligible kinetic energy and viscous dissipation of the mean flow; buoyancy only affects the mean flow; and equal exchange coefficients of all species and phases. With the exception of the last, these assumptions are either conditions of the experiments or are justified by successful use in the past.[6,7,20] The assumption of equal exchange coefficients of both phases is suspect wherever molecular transport is important, since molecular transport of finite-sized dispersed-phase elements is small.[6,7] However, molecular transport is not very important at the high Reynolds numbers of present flows; therefore, this approximation does not introduce serious limitations in comparison to the general uncertainties of LHF analysis for multiphase jets.

<u>Governing Equations</u>. Under the present assumptions, all scalar properties are only functions of the mixture fraction (mixture fraction is defined as the fraction of mass at a point which originated from the injector). This allowed use of the conserved-scalar formalism for scalar properties, similar to Lockwood and Naguib,[21] but based on mass-weighted (Favre) averages, following Bilger.[22]

Governing equations are solved for conservation of mass, streamwise mean momentum, mean mixture fraction, turbulence kinetic energy, rate of dissipation of turbulence kinetic energy, and mean-squared mixture fraction fluctuations (see Refs. 6, 7, 15 and 20 for the specific formulation and empirical constants). The present approach was successfully calibrated for a variety of constant and variable density single-phase round jets.[20] The formulation and constants, however, are not very different from those used by Lockwood and Naguib.[21]

Initial conditions for the calculations were specified at the injector exit, based on the LDA velocity measurements. It was found that the long injector passages yielded properties at the injector exit which were equivalent to fully-developed pipe flow. Rather than interpolate the measurement plane at x/d = 0.1, $\bar{u}$, k and ε were taken from Hinze[23] and Schlichting;[24] while $\bar{f} = 1$ and g = 0 by definition at the injector exit (note that Favre- and time-averaged quantities are identical for the single-phase flow at the injector exit).

Flow properties were uniform at the exit of the slug-flow injector, except for a narrow layer that could not be resolved using the LDA. In the constant property portion of the flow, $\bar{u}$ was known from the measurements; k was computed from measurements of $\overline{u'^2}$ and $\overline{v'^2}$, assuming $\overline{w'^2} = \overline{v'^2}$; and ε was approximated as $1.274 \times 10^{-4} \bar{u}^3/d$, similar to past work.[6,7] Properties in the boundary-layer along the wall were estimated for a range of L/d, bounding reasonable estimates of flow-development lengths, assuming clean entry and no vena

contracta. These properties were obtained from Schlichting.[24]

<u>State Relationships</u>. Under present assumptions, scalar properties are only functions of mixture fraction, called state relationships.[6,7] State relationships were found by straight-forward thermodynamic calculations for adiabatic mixing and equilibration of various mixtures of injected and ambient fluid. Calculations were completed for the limiting conditions of dry and water-vapor saturated ambient air. The effect of drop evaporation for dry air, however, was small; therefore, only a water-vapor saturated environment will be considered here.

When the ambient air is fully saturated, there is no tendency for the injected water to evaporate and the flow corresponds to an isothermal mixing process of the gas and liquid, each having constant densities. Thus, variable-density effects are only due to mixing of the phases under the LHF approximation. The state relationships for mixture density and liquid volume fraction are as follows:

$$\rho = (f/\rho_f + (1-f)/\rho_g)^{-1} \qquad (1)$$

$$\alpha_f = (1 + (\rho_f/\rho_g)(1-f)/f)^{-1} \qquad (2)$$

The state relationships were then used to find time- and Favre-averaged scalar properties, assuming a clipped Gaussian Favre-averaged probability density function for mixture fraction, similar to earlier work.[6,7,22]

<u>Numerical Solution</u>. The governing equations were solved using GENMIX.[25] The large density variations of the flows caused problems of computational stability and numerical accuracy, requiring much finer grids than are usually needed for single-phase flows. Present slug and fully-developed flow computations used 360 and 720 crosstream grid nodes with streamwise step sizes limited to 0.30 and 0.15 percent of current flow width, respectively. Doubling the number of grid nodes, in both the crosstream and streamwise directions, changed predictions less than one percent.

Results and Discussion

<u>Flow Visualization</u>. Typical flash photographs for fully-developed flow in the first wind-induced, second wind-induced and atomization breakup regimes are illustrated in Fig. 1. These results were obtained using the 9.5 mm diameter injector, however, findings for the 19.1 mm diameter injector were similar. Four pictures are shown for each test condition: near the injector exit; and centered at x/d = 50, 100 and 150. The lowest position appearing in the photographs is nearly 2m from the injector exit.

For first wind-induced breakup, the liquid surface exhibits fine-grained roughness near the injector exit, which becomes smoother, with large-scale irregularities appearing, far from the injector. This suggests shifts in the turbulence spectra of both phases. Liquid-phase turbulence properties near the injector exit are governed by the injector passage. Once the flow leaves the passage, however, mean liquid

velocities become more uniform since the gas cannot retard the surface velocity as effectively as the wall of the injector passage. This reduces turbulence production in the liquid, causing the turbulence to decay with the small-scale, high wave-number end of the spectrum disappearing first. The developing flow in the gas phase also favors the smallest scales near the injector exit. However, gas-phase turbulence probably does not have a strong influence on liquid surface properties at atmospheric pressure, since the gas density is small in comparison to the liquid. This was confirmed since the liquid surface exhibited little fine-grained roughness near the injector exit for slug flow, which had low initial turbulence intensities.[15] Thus, for present conditions, liquid-phase turbulence properties at the injector exit dominate roughness of the liquid surface, and probably influence drop size distributions once breakup occurs as well. For first wind-induced breakup, however, the large-scale irregularities (kinks) of the liquid column eventually cause breakup into the large liquid elements which are characteristic of this breakup regime.

In the second wind-induced breakup regime, the liquid-phase turbulence again produces small-scale surface roughness. However, these disturbances grow and are sheared from the surface, producing a cloud of drops surrounding the liquid core. The point where breakup begins is roughly three injector diameters from the injector exit for the condition illustrated in Fig. 1. The character of the surface roughness influences breakup, e.g., slug flow conditions at the same flow rate, where the liquid surface was relatively smooth, caused the point of breakup to move downstream to 25-30 injector diameters from the exit.[15] Present criteria for breakup regime transitions do not account for effects of flow development at the injector exit, which clearly affect the onset of atomization: extending the criteria to account for these effects is clearly needed. In spite of breakup at the surface, however, an all-liquid core can clearly be seen in the flow. This liquid core eventually breaks up far from the injector, probably yielding some rather large drops, similar to first wind-induced breakup.

As noted earlier, increasing injector velocities in the second wind-induced breakup regime cause the point of breakup of the surface of the liquid column to move toward the injector exit. When breakup reaches the exit, the atomization breakup regime is entered and is observed for all higher injector flow rates. The atomization condition illustrated in Fig. 1 is well within the atomization regime. The wispy appearance of the drop-containing region near the edge of the flow, similar to a single-phase flow containing tracer particles, suggests that the drops near the exit are small. Clear areas of drop intermittency, also similar to single-phase turbulent shear layers, penetrate the drop-containing region. The extent of penetration is relatively small near the injector exit, suggesting the presence of an all-liquid core similar to the other breakup regimes illustrated in Fig. 1. The depth of penetration of the drop-free regions increases with increasing distance from the injector, but drop intermittency is not seen at the axis until x/d ~ 150-200.

The spray had a more opaque, milky appearance for slug flow than for fully-developed flow and atomization breakup,

suggesting higher concentrations of smaller drops in the drop-containing shear layer.[15] However, the rate of spread of the shear layer (indicated by the extent of the region where drops scattered significant light on the photographs) was significantly smaller and the appearance of drop intermittency along the axis was delayed for slug flow. This implies a longer all-liquid core for slug flow than for fully-developed flow, for the same injector flow rate. This behavior is confirmed by the liquid volume fraction measurements to be considered next.

Mean Liquid Volume Fractions. Measured and predicted time-averaged mean liquid volume fractions along the axis of the fully-developed and slug-flow sprays are plotted as a function of x/d in Figs. 2 and 3. Fully-developed flows included 9.5 and 19.1 mm diameter injectors and all three breakup regimes. Slug flows were limited to the 9.5 mm diameter injector and the second wind-induced and atomization breakup regimes.

For fully-developed flow (Fig. 2), the near-injector region (x/d < 10) exhibits liquid volume fractions near unity. For x/d > 10, however, liquid volume fractions decrease rapidly in the second wind-induced and atomization breakup regimes, reaching values of 0.2-0.3 at x/d = 150. For x/d < 40, the measurements in the second wind-induced and atomization regimes are similar, when the streamwise distance is normalized by the injector diameter. This behavior suggests a turbulent mixing-controlled process in the near-injector region, which might be amenable to analysis using the LHF approximation.

In contrast, mixing is much slower for the first wind-induced breakup regime than the other breakup regimes illustrated in Fig. 2 for fully-developed flow. In this case, liquid volume fractions remain near unity for x/d < 50, followed by a region of rapid reduction of mean liquid volume fractions along the axis. In the region where the mean liquid volume fraction declines, however, apparent mixing is only due to lateral deflection of the liquid column (the formation of kinks and lateral flapping of the column as a whole), rather than the more complete mixing caused by the formation of drops, see Fig. 1. However, flow properties for first wind-induced breakup are seen to also scale with injector diameter.

The results illustrated in Fig. 2 superficially suggest a relatively short all-liquid core near the injector exit, particularly for second wind-induced and atomization breakup. This is not actually the case. Due to the large water/air density ratio of the flow, liquid volume fraction is a very sensitive function of mixture fraction. This can be seen from the following table, giving α_f as a function of f, under the LHF approximation for the present density ratio (846:1).

f	1.0000	0.9999	0.9990	0.9900	0.9000
α_f	1.000	0.922	0.541	0.105	0.011

It can be seen that mixture fraction decreases only 1 percent while liquid volume fraction decreases by a factor of

ten, from 1 to 0.1. Thus, all the results illustrated in Fig. 2 represent mixture fractions greater than 0.99. (Note that with liquid velocities greater than gas velocities, the reduction of f would be even smaller if the LHF approximation was not valid.) Thus, as expected, mixing is much slower for the present liquid jets than for single-phase flows, where $\tilde{f}_c \sim$ 0.03 at x/d = 150:[12] long liquid cores are present for all flows considered here, when viewed in terms of mixture fraction.

LHF predictions are essentially independent of Reynolds number for the high Reynolds numbers of present tests; therefore, the single prediction appearing in Fig. 2 represents all test conditions for fully-developed flow. Measurements for second wind-induced breakup are in good agreement with this prediction for x/d < 40 while similar agreement is observed for atomization breakup when x/d < 100. At greater distances, measured liquid volume fractions are greater than predictions, suggesting increased effects of relative velocities between the phases. It is plausible that results for second wind-induced breakup depart from predictions sooner than atomization breakup, since drop sizes are larger for second wind-induced breakup, providing greater potential for significant relative velocities between the phases. Failure of the LHF approximation also occurs slightly sooner (in terms of x/d) for the smaller injector, since smaller passage diameters yield higher flow deceleration rates (which scales as u_o/d),[6,7] which cause higher relative velocities in the flow. Such higher relative velocities become significant in comparison to local flow velocities nearer to the injector, reducing the region where the LHF approximation is adequate. These effects eventually become important for all the flows considered in Fig. 2, causing LHF predictions to fail far from the injector, as the dilute spray region is approached. This observation is consistent with deficiencies reported in the past for LHF analysis of dilute sprays.[6,7]

Comparing results for atomization breakup for fully-developed and slug flow at the injector exit (cf., Figs. 2 and 3) shows that effects of flow development at the injector exit are nearly as dramatic as effects of the breakup regime. The physical reason for this behavior is that the liquid density is large in comparison to the gas; therefore, fully-developed flow carries significant levels of turbulence energy into the flow, enhancing mixing in the region where mixture fractions are high. As noted earlier, this liquid-phase turbulence also creates instabilities in the liquid surface which would provide more rapid breakup of liquid into drops – enhancing mixing as well.

These effects cause slower initial rates of flow development for slug flow than for fully-developed flow, e.g., liquid volume fractions for slug flow remain near unity for x/d < 50, as opposed to x/d < 10 for fully-developed flow. However, later development of the flow is rapid, resulting in mean liquid volume fractions near 0.3 at x/d = 150. This implies a relatively long all-liquid core, particularly when viewed in terms of mixture fraction – as noted earlier.

Predictions illustrated in Fig. 3 are relatively independent of Reynolds number, but are strongly influenced by the degree of flow development at the injector exit (which is represented by the passage L/d). It is encouraging that computations for L/d = 0 and 5, which are reasonable limits for the test injector, tend to bound the measurements for atomization breakup. Comparing results for atomization breakup in Figs. 2 and 3 shows that LHF predictions properly represent the strong effect of the degree of flow development at the injector exit on the subsequent mixing of the spray in the near-injector region. The effect of flow development is probably a contributing factor in controversies concerning the properties of the all-liquid core based on measurements from short L/d injectors.[3-5]

Radial profiles of time-averaged liquid volume fractions for atomization breakup are illustrated in Figs. 4-6. Measurements and predictions are plotted as a function of radial distance, normalized by the injector diameter, at various distances from the injector exit. Results for fully-developed flow for the 19.1 and 9.5 mm diameter injectors are plotted in Figs. 4 and 5, similar results for slug flow appear in Fig. 6.

The apparent flow widths seen in Figs. 4-6 are unusually narrow in comparison to single-phase jets. For example, flow widths are on the order of 2r/d = 4-6 for x/d = 100-150, which correspond to r/x on the order of 0.02. In comparison, widths of single-phase jets are nearly an order-of-magnitude larger, ca. $r/x = 0.15.$[26] The sensitivity of liquid volume fraction to mixture fraction, mentioned earlier, is the main cause of this behavior, e.g., based on Eq. (2), profiles of mixture fraction are much wider than liquid volume fraction. The extended all-liquid core for present flows also contributes to this behavior, since liquid that has not become atomized cannot mix very effectively.

For fully-developed flow, the comparison between predicted and measured radial profiles of mean liquid volume fractions seen in Figs. 4 and 5 can be anticipated from the results along the axis illustrated in Fig. 2. Conditions where $\bar{\alpha}_{fc}$ is predicted well, e.g. x/d < 100, also result in reasonably good predictions of radial profiles. All predictions far from the injector, however, overestimate the width of the flow. This agrees with past evaluations of LHF analysis in the dilute portions of sprays, which showed that the method invariably overestimates measured rates of flow development.[6,7,12-14] This occurs since relative velocities become significant whenever flow velocities are low, which roughly corresponds to the dilute-spray region.

Results for slug flow are illustrated in Fig. 6. In this case predictions are plotted for the limits of L/d = 0 and 5. Near the injector, there is a reasonably wide zone where liquid volume fractions are nearly unity. Predictions suggest a sharp transition between this region and the shear layer, while measurements show a more gradual transition between these regions. This discrepancy is partly due to gradient-broadening errors of the measurements, where the finite diameter of the paths of the absorption measurements cannot resolve rapid radial variations of mean liquid volume fractions. On the other hand, the discontinuity of the predictions is due to approximations made to match calculations in the shear layer with the all-liquid core, and is probably not observed in nature.

The discrepancies between predictions and measurements are largest at x/d = 100 for slug flow. Both predictions underestimate the flow width, rather than overestimating it, which is the expected behavior of the LHF approximation. This behavior is caused by the discrepancies between measured $\bar\alpha_{fc}$ and predictions for the limits of L/d = 0 and 5 near x/d = 100 (see Fig. 3). Thus, the poor agreement at x/d = 100 is due largely to the $\bar\alpha_f/\alpha_{fc}$ normalization used in Fig. 6.

For slug flow and x/d = 150, corresponding to low values of $\bar\alpha_{fc}$, the predictions for L/d = 0 and 5 overestimate the development of the jet, similar to fully-developed flow. However, the slug flow predictions do not depart as much from the measurements as for the fully-developed flow at this position (see Fig. 5). Two reasons can be forwarded for this behavior. First of all, slug flow develops more slowly than fully-developed flow, providing a more extended shear layer region with lower rates of deceleration – tending to favor the LHF approximation. Secondly, as noted earlier, it appeared that smaller drops were generated for slug flow than for fully-developed flow, which also favors the LHF approximation. Based on the Taylor[27] breakup criterion, discussed by Reitz and Bracco,[2] the production of smaller drops for slug flow than fully-developed flow is plausible because of the higher velocity gradients near the liquid surface. However, direct measurements of drop size and velocity properties in the near-injector region are needed to provide more information concerning these conjectures.

Entrainment Rates. The entrainment rate of a jet is proportional to the rate of increase of the jet mass flow rate with distance from the injector and is a good measure of the turbulent mixing properties of the flow.[28] Measured and predicted entrainment rates for the present flows are illustrated in Fig. 7. Normalized entrainment rates are plotted as a function of distance from the injector, considering all three breakup regimes for fully-developed flow, and second wind-induced and atomization breakup for slug flow. As noted earlier, present predictions did not vary significantly with Reynolds number; therefore, the predictions illustrated in Fig. 7 are representative of the Reynolds number range of the experiments. As before, predictions at the limits of L/d = 0 and 5 were made for slug flow, however, the results were nearly the same; therefore, only a single prediction line appears in Fig. 7. The entrainment rate correlation of Ricou and Spalding[28] is also plotted in Fig. 7: this correlation was developed for fully-developed flow (x/d > 20) of variable-density turbulent gas jets.

Measured normalized entrainment rates increase with increasing distance from the injector. The entrainment rates for first wind-induced breakup are substantially lower than for second wind-induced breakup and atomization, which differ only slightly from each other. This is plausible, since the liquid column for first wind induced-breakup does not shatter into drops for the present test range; therefore, there is little surface area available to promote momentum exchange and turbulent mixing.

In general, predictions substantially overestimate measurements for all the results illustrated in Fig. 7. Furthermore, the correlation of Ricou and Spalding[28] yields much larger estimates of entrainment than present measurements and predictions. This is due to effects of both flow development and finite relative velocities. Differences between the correlation of Ref. 28 and present LHF predictions are a measure of effects of flow development. This is caused by differences between present velocity and density distributions in the developing flow near the injector and velocity profiles for fully-developed turbulent gas jets, which have rather modest density variations in the fully-developed region of the flow. In the terminology of integral theories, this is a shape-factor effect, resulting from dissimilar velocity and scalar property profiles. Similarity in this sense implies invariance of radial profiles when normalized by centerline quantities and plotted as a function of r/x: the results illustrated in Figs. 4-6 show that this requirement is not satisfied for the present flows – even for atomization breakup.

Present predictions allow for effects of flow development, but still significantly overestimate measured rates of entrainment. The discrepancies are smallest for fully-developed flow and atomization breakup, but even this prediction is not very satisfactory. This behavior follows since entrainment rates are strongly influenced by flow properties near the edge of the flow, where velocities are low and effects of relative velocities become important. Stated differently, the periphery of the flow, which directly affects entrainment properties, is a dilute-spray region where LHF analysis invariably overestimates rates of flow development, which is represented by properties like the entrainment rate. Similar deficiencies are less apparent for liquid volume fractions, since present measurements emphasize regions having high mixture fractions. Flow velocities are also high in these regions, tending to reduce errors due to finite relative velocities.

Sensitivity Study. The sensitivity of present calculations was examined similar to past evaluations of spray analysis.[13,14] Predictions were most sensitive to uncertainties in the initial values of k and ε.[15] However, these parameters were reasonably well known for fully-developed injector flows, while affects of turbulence properties in the core of the flow were not very significant for slug flow. Thus, uncertainties in predictions, aside from well-recognized limitations of k-ε turbulence models for boundary-layer flows, are generally within experimental uncertainties.

A final point should be mentioned with respect to the turbulence model. If the present flows formally satisfied the LHF approximation, they would represent a variable density jet with a density ratio of ca. 1000:1. This is roughly two orders of magnitude greater than the variable-density single-phase flows which were used to calibrate the present Favre-averaged turbulence model.[20] Thus, whether these methods can accurately handle the present large density ratios if the LHF assumption was formally satisfied is unknown and deficiencies here could have contributed to discrepancies between predictions and measurements. Based on present findings, however,

limitations of the LHF approximation due to finite relative velocities in low mean-velocity regions of the flow (the dilute-spray region) appear to be a more obvious source of errors in the predictions.

Conclusions

Major conclusions of the study are as follows:

1. Pressure-atomized sprays are unusually sensitive to the degree of flow development and turbulence levels at the injector exit: fully-developed turbulent flows cause much faster rates of flow development and shorter all-liquid cores than slug flows having low initial turbulence intensities.

2. Locally-homogeneous flow analysis was reasonably successful for atomization breakup, in the dense-spray, near-injector region where mean liquid volume fractions are relatively high ($\bar{\alpha}_f > 0.2$). In particular, present methods provided good estimates of the striking effects of flow development at the injector exit, in spite of the large density variations (ca. 1000:1) of the flows.

3. Similar to past findings in this laboratory,[10-14] the LHF approximation was less effective for properties of the dilute-spray region near the periphery of the flow and far downstream from the injector. This deficiency caused flow entrainment rates to be underestimated in the region observed (x/d < 150).

4. Properties of the all-liquid core near the injector exit are influenced by the breakup regime and the state of flow development at the injector exit: the last effect is probably a factor causing differences in all-liquid core lengths reported by various workers.[3-5]

Present conclusions are based on large-scale sprays (9.5 and 19.1 mm injector diameters) which have much lower flow deceleration rates than practical injectors – favoring use of the LHF approximation. Present results were also limited to water injected into air at normal temperature and pressure: other liquids and ambient gases will modify drop-size distributions and probably the effectiveness of the LHF approximation as well. Additional study of this important and fundamental multiphase flow is clearly needed.

References

[1]Ranz, W. E., "Some Experiments on Orifice Sprays," Can. J. Chem. Engr., Vol. 36, August 1958, pp. 175-181.

[2]Reitz, R. D. and Bracco, F. V., "Mechanism of Atomization of a Liquid Jet," Phys. Fluids, Vol. 25, October 1982, pp. 1730-1742.

[3]Chehroudi, B., Onuma, Y., Chen, S.-H. and Bracco, F. V., "On the Intact Core of Full-Cone Sprays," SAE Paper No. 850126, 1985.

[4]Hiroyasu, H., Shimizu, M. and Arai, M., "The Breakup of a High Speed Jet in a High Pressure Gaseous Environmment," ICLASS-82, University of Wisconsin, Madison, Wisconsin, 1982.

[5]Phinney, R. E., "The Breakup of a Turbulent Liquid Jet in a Gaseous Atmosphere," J. Fluid Mech., Vol. 60, October 1973, pp. 689-701.

[6]Faeth, G. M., "Evaporation and Combustion in Sprays," Prog. Energy Combust. Sci., Vol. 9, 1983, pp. 1-76.

[7]Faeth, G. M., "Mixing, Transport and Combustion in Sprays," Prog. Energy Combust. Sci., in press.

[8]Wu, K.-J., Su, C.-C., Steinberger, R. L., Santavicca, D. A. and Bracco, F. V., "Measurements of the Spray Angle of Atomizing Jets," J. Fluids Engr., Vol. 105, December 1983, pp. 406-415.

[9]Wu, K.-J., Coghe, A., Santavicca, D. A. and Bracco, F. V., "LDV Measurements of Drop Velocity in Diesel-Type Sprays," AIAA J., Vol. 22, September 1984, pp. 1263-1270.

[10]Mao, C.-P., Wakamatsu, Y. and Faeth, G. M., "A Simplified Model of High Pressure Spray Combustion," Eighteenth Symposium (International) on Combustion, The Combustion Institute, Pittsburgh, 1981, pp. 337-347.

[11]Mao, C.-P., Szekely, G. A., Jr. and Faeth, G. M., "Evaluation of a Locally Homogeneous Flow Model of Spray Combustion," J. Energy, Vol. 4, March-April 1980, pp. 78-87.

[12]Shearer, A. J., Tamura, H. and Faeth, G. M., "Evaluation of a Locally Homogeneous Flow Model of Spray Evaporation," J. Energy, Vol. 3, September-October 1979, pp. 271-278.

[13]Solomon, A.S.P., Shuen, J.-S., Zhang, Q.-F. and Faeth, G. M., "Structure of Nonevaporating Sprays: I. Near-Injector Conditions and Mean Properties," AIAA J., Vol. 23, October 1985, pp. 1548-1555.

[14]Solomon, A.S.P., Shuen, J.-S., Zhang, Q.-F. and Faeth, G. M., "Structure of Nonevaporating Sprays: II. Drop and Turbulence Properties," AIAA J., Vol. 23, November 1985, pp. 1724-1730.

[15]Ruff, G. A. and Faeth, G. M. "Dense-Spray Structure and Phenomena: Part II. Pressure-Atomized Sprays," Interim Report under Grant No. AFOSR-85-0244, The University of Michigan, Ann Arbor, Michigan, September 1987.

[16]Smith, R. H. and Wang, C.-T., "Contracting Cones Giving Uniform Throat Speeds," J. Aero. Sci., Vol. 11, October 1944, pp. 356-360.

[17]Santoro, R. J., Semerjian, J. H., Emmerman, P. J. and Goulard, R., "Optical Tomography for Flow Field Diagnostics," Int. J. Heat Mass Trans., Vol. 24, July 1981, pp. 1139-1150.

[18]Gomi, H. and Hasegawa, K. I., "Measurements of the Liquid Phase Mass in Gas-Liquid Sprays by X-ray

Attenuation," Int. J. Multiphase Flow, Vol. 10, December 1984, pp. 653-662.

[19]Miesse, C. C., "Correlation of Experimental Data on Disintegration of Liquid Jets," Ind. Engr. Chem., Vol. 47, September 1955, pp. 1690-1697.

[20]Jeng, S.-M. and Faeth, G. M., "Species Concentrations and Turbulence Properties in Buoyant Methane Diffusion Flames," J. Heat Trans., Vol. 106, August 1985, pp. 721-727.

[21]Lockwood, F. C. and Naguib, A. S., "The Prediction of Fluctuations in the Properties of Free, Round-Jet Turbulent Diffusion Flames," Combust. Flame, Vol. 24, February 1975, pp. 109-124.

[22]Bilger, R. W., "Turbulent Jet Diffusion Flames," Prog. Energy Combust. Sci., Vol. 1, 1976, pp. 87-109.

[23]Hinze, J. O., Turbulence, 2nd ed., McGraw-Hill, New York, 1975, p. 427 and pp. 724-734.

[24]Schlichting, H., Boundary Layer Theory, 7th ed., McGraw-Hill, New York, 1979, p. 599.

[25]Spalding, D. B., GENMIX: A General Computer Program for Two-Dimensional Parabolic Phenomena, Pergamon Press, Oxford, 1977.

[26]Wygnanski, I. and Fiedler, H. E., "Some Measurements in the Self-Preserving Jet," J. Fluid Mech., Vol. 38, September 1969, pp. 577-612.

[27]Taylor, G. I., "Generation of Ripples by Wind Blowing Over a Viscous Fluid," Collected Works of G. I. Taylor, Vol. 3, 1940, pp. 244-254.
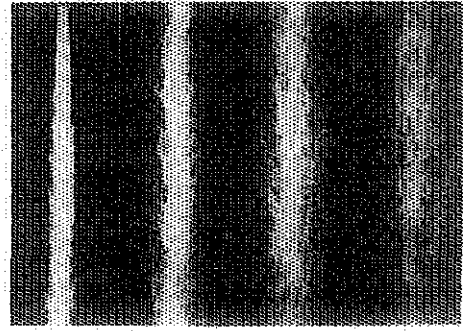
[28]Ricou, F. P. and Spalding, D. B., "Measurements of Entrainment by Axisymmetrical Turbulent Jets," J. Fluid Mech., Vol. 11, August 1961, pp. 21-32.
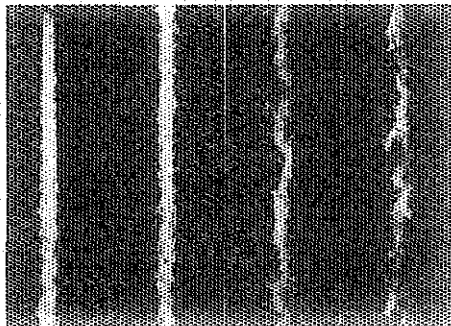
(1c) Atomization breakup.

Fig. 1   Flash photographs for the 9.5 mm diameter injector and fully-developed flow:
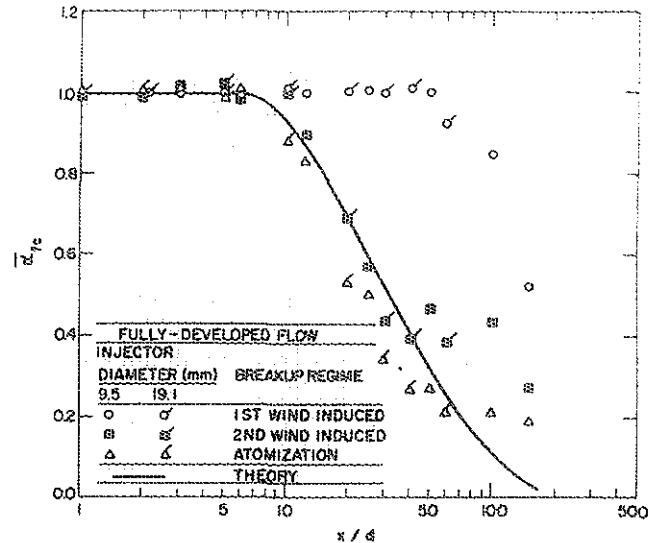

Fig. 2   Time-averaged liquid volume fractions along the axis for fully-developed flow.
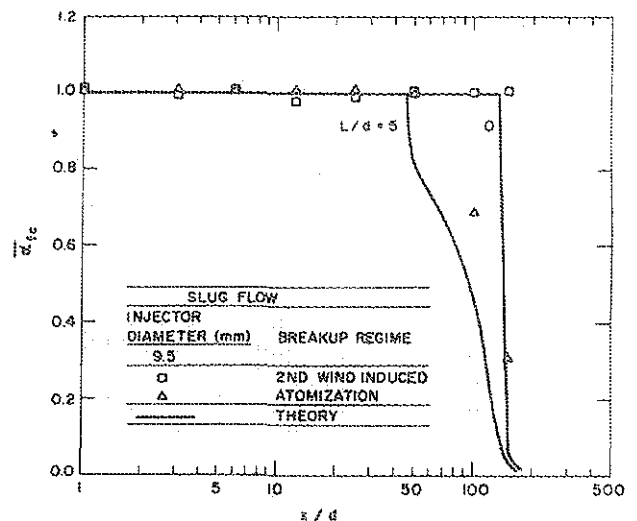

Fig. 3   Time-averaged liquid volume fractions along the axis for slug flow.

(1a) First wind-induced breakup;
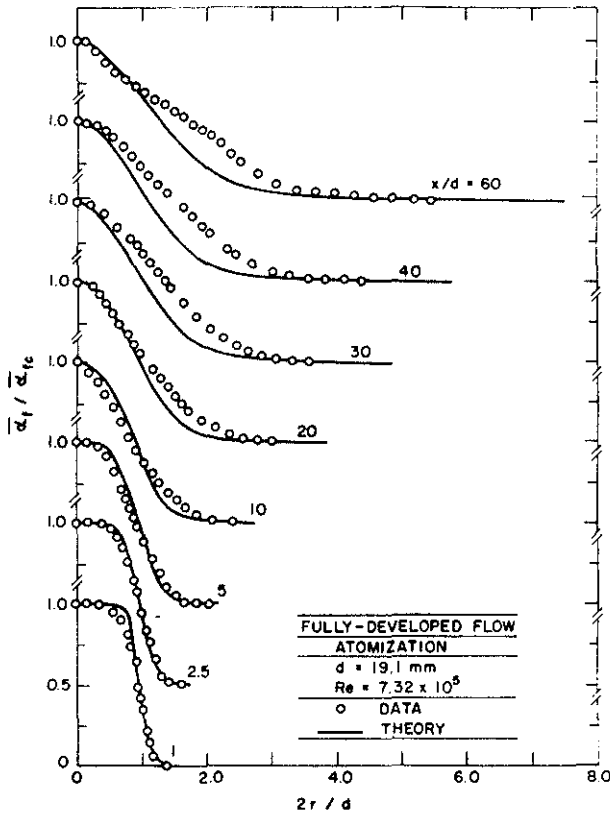

(1b) Second wind-induced breakup;

Fig. 4   Radial profiles of time-averaged liquid volume fractions for fully-developed flow and atomization breakup (19.1 mm diameter injector).
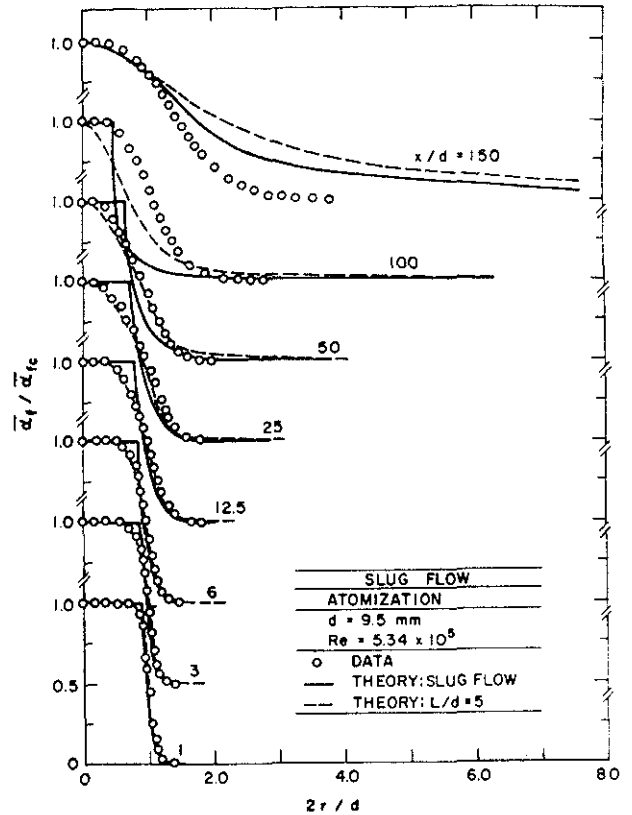

Fig. 6   Radial profiles of time-averaged liquid volume fractions for slug flow and atomization breakup (9.5 mm diameter injector).
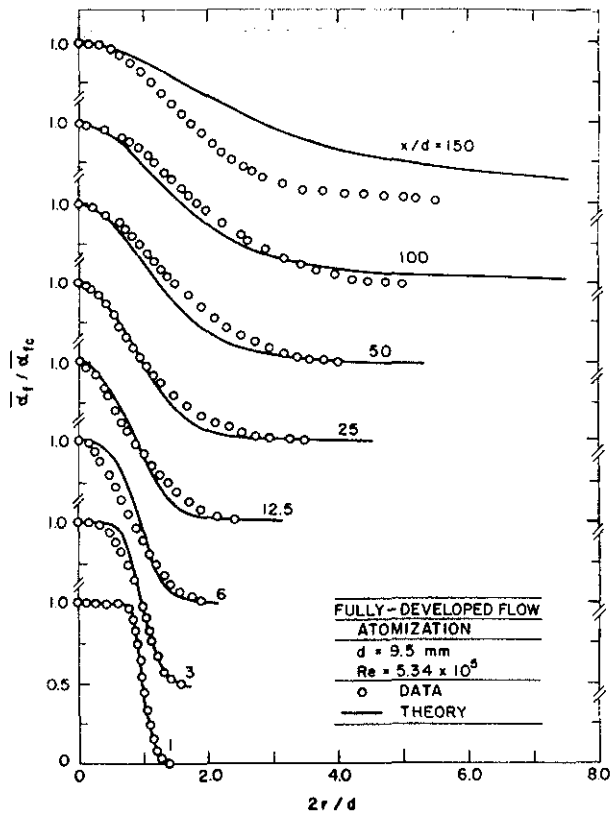

Fig. 5   Radial profiles of time-averaged liquid volume fractions for fully-developed flow and atomization breakup (9.5 mm diameter injector).
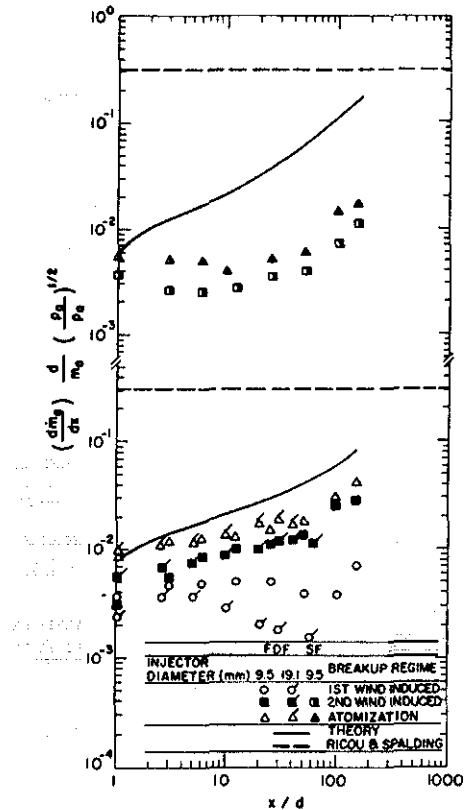

Fig. 7   Entrainment rates as a function of distance from the injector.

10